

Article

Effect of Nitrogen Content on the Formation of Inclusions in Fe-5Mn-3Al Steels

Michelia Alba , Muhammad Nabeel and Neslihan Dogan

Department of Material Science and Engineering, McMaster University, 1280 Main Street West, Hamilton, ON L8S 4L7, Canada; nabeelm@mcmaster.ca (M.N.); dogann@mcmaster.ca (N.D.)

* Correspondence: albam@mcmaster.ca

Received: 24 August 2020; Accepted: 17 September 2020; Published: 18 September 2020



Abstract: The effect of N content on the characteristics and formation of inclusions in the Fe-5Mn-3Al steels was investigated in this study. Two synthetic steel melts were produced by two different methods—N₂ gas purging and injecting—to introduce nitrogen into the melt. The N content of steel melt varied from 2 to 54 ppm. An increase in the N content to 47 ppm (for 533N-P) and 58 ppm (for 533N-I) increased the total amount of inclusions from 13 to 64 mm^{−2} and from 21 to 101 mm^{−2}, respectively. The observed inclusions were Al₂O_{3(pure)}, Al₂O₃-MnS, AlN_(pure), AlN-MnS, AlON, AlON-MnS, and MnS. When the N content was less than 10 ppm, AlN-MnS inclusions were the primary type of inclusions and they formed as solidification products. With an increase in the N content, AlN_(pure) inclusions became the dominant type of inclusions as AlN was stable in the liquid steel. These findings were confirmed by thermodynamic calculations. The influence of cooling rate on the types of inclusions was studied and a higher number of AlN-MnS inclusions were observed in samples with slow cooling rate.

Keywords: AlN inclusions; ASPEX; inclusion analysis; medium manganese steel; nitrogen; scanning electron microscope; co-precipitation

1. Introduction

Among the third generation of Advanced High Strength Steel (AHSS), medium manganese steels are becoming more popular because they have a high tensile strength similar to that of high manganese steels while having reduced production cost [1]. Medium manganese steels are preferred over the high manganese steels because of problems associated with continuous casting due to poor hot ductility of high manganese steels [2–4]. This poor hot ductility is caused by the precipitation of inclusions (e.g., AlN) in the steel [3]. The presence of inclusions in steel is known for their adverse impact on the mechanical properties of the steel and the information regarding the characteristics of inclusions (such as their size, morphology, and composition) in medium manganese steels is limited [3,5–13]. Notably, the influence of the alloying elements on the formation of inclusions in the medium manganese steel is not well known [5,8]. The authors [14,15] investigated the effect of Mn and Al contents in liquid steel on the formation of inclusions. They found that with an increase in the Mn content, the number of inclusions increased, particularly AlN and MnS inclusions [14]. It was justified by the fact that manganese content can increase the solubility of nitrogen in the steel [16,17]. Moreover, it was also found that with increasing Al content from 0.5% to 6% in the medium manganese steel (~5% Mn), the total number of inclusions also increased 2.5 times, especially the number of AlN inclusions which increased from 2 mm^{−2} to around 20 mm^{−2} [15].

Liu et al. [18] investigated the formation of AlN inclusions in high manganese steel (Fe-25Mn-3Al-3Si) produced in electroslag remelting (ESR) and argon oxygen decarburization (AOD) processes with a nitrogen content of 6 and 24 ppm, respectively. They reported that the AlN inclusions

observed in ESR steel (6 ppm N) formed during the solidification process and the AlN inclusions found in AOD steel (24 ppm N) formed in liquid steel during cooling. Xin et al. [19] also observed AlN inclusions in high manganese steel (Fe-17Mn-2Al-0.6C) with N content of 43 ppm. The calculated formation temperature of AlN in the steel was around 9 degrees lower than the liquidus temperature [19], which suggests that AlN inclusions were formed in the mushy zone during solidification of steel. Thus, the formation behavior of AlN inclusions depends on the N content of steel, i.e., AlN inclusions can be solidification products in low N containing steels [20] or they can form during the refining of liquid steel with high nitrogen content [18,21]. The inclusions that are formed as a solidification product usually exist in small sizes [22]. On the other hand, the inclusions which form in liquid steel can grow to a larger size or agglomerate with other inclusions. Thus, a difference in the size distribution of AlN inclusions formed at different N contents can be expected. Moreover, AlN inclusions exhibit different morphologies. In the previous studies [9,23–25], the morphology of AlN inclusions has been reported as hexagonal [9], plate-like [24], rod [9] or needle-like [23], and dendritic [25] form. To the authors' knowledge, there is no systematic study on the effect of N content on the characteristics of inclusions and their formation behavior in medium Mn steel.

Therefore, this study aims at investigating the influence of N content on the formation of inclusions in medium Mn steels. For this, two experimental steel melts were produced in the laboratory by introducing N₂ gas into steel through different methods. Both steel melts were investigated for variation in the characteristics of inclusions, i.e., their number density, composition, size, and morphology. Furthermore, the formation mechanism of inclusions is discussed, considering the characteristics of inclusions and thermodynamics.

2. Materials and Methods

A resistance-heated vertical tube furnace was used to produce synthetic steel containing Fe-5Mn-3Al-3Si-0.1C. A schematic diagram of the experimental set up is shown in Figure 1. Before heating, the furnace chamber was evacuated and backfilled with high purity Ar gas (99.999%) at a flow rate of 500 mL/min. The oxygen content in Ar gas was reduced by passing it through Ti turnings at 923 K. The steel material was charged in an alumina crucible and heated to 1873 K. Two experiments were set up using different methods for introducing N₂ gas into the molten steel. In both experiments, the furnace chamber was evacuated after reaching the target temperature. In the first experiment (533N-P), the chamber was backfilled by purging a mixture of Ar and N₂ gas (1:1). After 180 min, the mixing ratio was changed to Ar:N₂ = 1:2. In the second experiment, after the evacuation, the chamber was backfilled with only Ar gas (500 mL/min), and N₂ gas was introduced by injecting it into the molten steel bath by using alumina tube at a rate of 300 mL/min. The alumina tube was at the height of 1.5 cm from the bottom of the crucible, i.e., almost in the center of the molten steel bath. This set of experiments is denoted as 533N-I. In this experiment, N₂ gas was purged directly from a gas cylinder (99.999% N₂) without passing through Ti turnings, see Figure 1. In both experiments, several pin samples were taken to monitor the N content in the steel melts. The sampling sequence is shown in Table 1. The first sample (S1) was taken before introducing N₂ gas in the system. All the pin samples were air-cooled, while the remaining bulk steel was cooled along with the furnace, at a cooling rate of 0.167 K/s. In the case of the 533N-P experiment, there is a 180 min gap between S4 and S5 samples. Several samples were taken between S4 and S5; however, there was no significant change in the N content during that holding time. So, the samples shown in Table 1 were chosen to represent the considerable variation in the N content of steel melt.

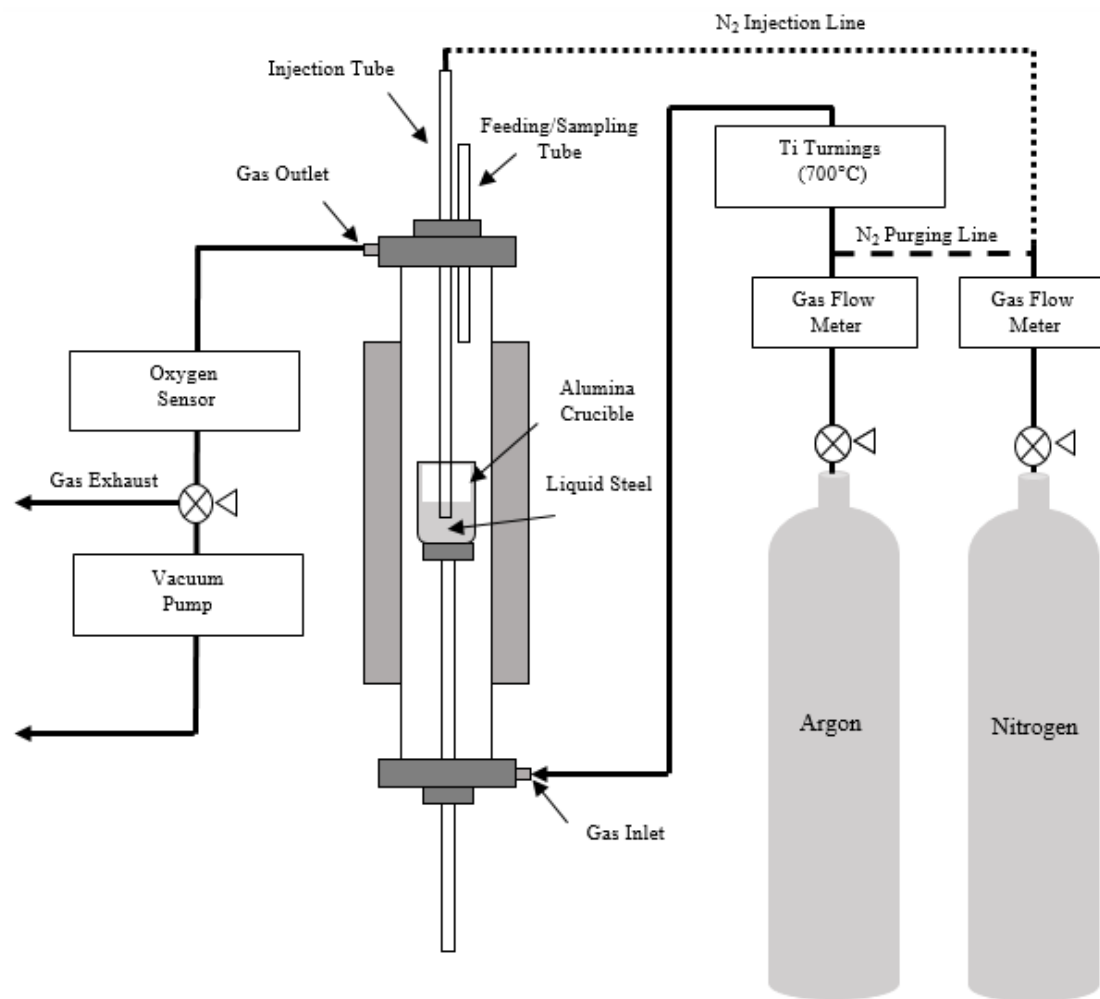


Figure 1. Schematic diagram of the experimental set-up used in this study.

Table 1. Experimental steps.

533N-P							533N-I						
Gas	Purge Ar:N ₂ = 1:1			Purge Ar:N ₂ = 1:2			Gas	Purge Ar Inject N ₂					
Samples	S1	S2	S3	S4		S5	S6	S1	S2	S3	S4	S5	
Time (min)	0	15	45	90	180	270	300	0	10	15	30	60	

The oxygen-nitrogen and carbon-sulfur contents of samples were measured by commercial LECO Oxygen/Nitrogen (ON736)TM [26] and LECO Carbon/Sulfur (CS744)TM [27] analyzer, respectively. The chemical analysis of steel samples was conducted by induction coupled plasma optical emission spectrometry (ICP-OES). The steel samples were analyzed for inclusions by using an automated scanning electron microscope (SEM) equipped with an ASPEXTM [28] feature, which is a commercial system for inclusion analysis. The following parameters were used: magnification—356x, accelerating voltage—20 kV, emission current—43.4 μ A, and spot size—35%. The analyzed area and the total number of detected inclusions varied from 10 to 42 mm² and around 330 to 2943, respectively. In this study, the inclusions having a maximum diameter (D_{max}) > 2 μ m were detected. All the inclusions were classified into four major inclusion classes, which are Al₂O₃, AlN, MnS, and Other. Furthermore,

the Al_2O_3 class was divided into two subclasses, $\text{Al}_2\text{O}_{3(\text{pure})}$ and $\text{Al}_2\text{O}_3\text{-MnS}$. In the case of AlN , it had four subclasses, which were $\text{AlN}_{(\text{pure})}$, AlN-MnS , AlON-MnS , and AlON . The ‘Other’ class contained complex oxide inclusions besides the aforementioned classes. The details of the inclusion classification were described elsewhere [14].

3. Results

3.1. Chemical Composition of the Steels

The chemical composition of the steel samples is listed in Table 2. The nitrogen content of the 533N-P steel samples increased with the holding time. For $\text{Ar:N}_2 = 1:1$, the highest value of N content was measured in S4. An increase in the N_2 ratio in the gas mixture ($\text{Ar:N}_2 = 1:2$) resulted in a maximum value of 54 ppm after 270 min (S5). However, the N content in the 533N-I steel reached 54 ppm only after 10 min of injecting N_2 gas into the steel melt, and it remained almost constant throughout the experiment. The O content of the samples of 533N-I steel was higher, especially for samples taken at 10 and 15 min. These high values could be the result of oxygen impurities in N_2 gas, which was injected into the steel melt. N_2 gas was not passed through the titanium turning in the 533N-I experiment. The results from the LECO analyzer will have a deviation of around ± 2 ppm while the elemental analysis using ICP-OES has a relative standard deviation (RSD) of less than 5%.

Table 2. The chemical composition of the steel melts.

Steel Set	Sample	Time (min)	Mn (%)	Al (%)	Si (%)	C (%)	S (%)	N (ppm)	O (ppm)
533N-P	S1	0	4.96	2.63	3.77	0.103	0.0028	2	14
	S2	15						23	3
	S3	45						33	9
	S4	90						47	2
	S5	270						54	2
	S6	300						52	3
533N-I	S1	0	4.77	2.74	4.12	0.102	0.0027	-	4
	S2	10						54	16
	S3	15						54	25
	S4	30						-	-
	S5	60						54	11

3.2. Characteristics of Inclusions

Figure 2 presents the number per unit area of inclusions (N_A) observed in samples taken during the two experiments. It could be seen that sample S1, which was taken before introducing N_2 gas to the steel melt, contained 13 mm^{-2} and 21 mm^{-2} of inclusions in 533N-P and 533N-I steel, respectively. In sample S1 from 533N-P, the Al_2O_3 inclusions counted for almost 80%, and the rest of the inclusions were AlN . While, before N_2 gas injection in 533N-I steel melt, it contained ~40% of Al_2O_3 and AlN inclusions each. In 533N-P steel melt, the N_A value of inclusions gradually increased from 13 to 64 mm^{-2} as the N content of steel reached 47 ppm (after 90 min of N_2 gas purging in the system). Thereafter, the N_A value remained almost constant with increasing holding time despite a slight increase in the N content of steel (to more than 50 ppm). The N_A value of Al_2O_3 inclusions decreased from 10 to less than 1 mm^{-2} , while the N_A value of AlN inclusions substantially increased from 3 to 62 mm^{-2} . The number of MnS and ‘Other’ inclusions were generally low, i.e., < 5% of total inclusions.

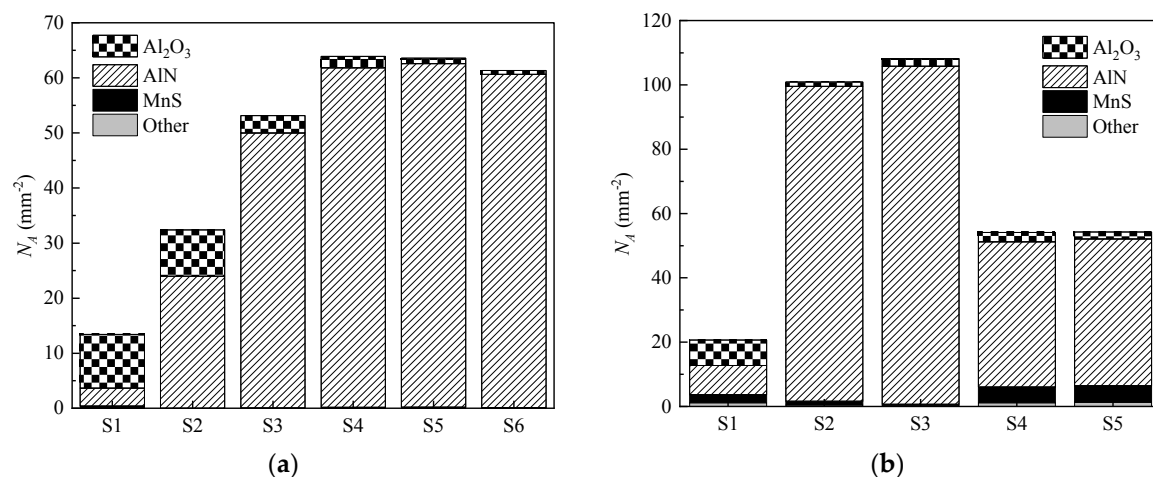


Figure 2. The total number of inclusions per unit area (N_A) and their composition detected in (a) 533N-P and (b) 533N-I steel melts.

Similar to 533N-P, a significant increase in the N_A of inclusions was observed in 533N-I steel samples after injection of N_2 gas in the steel melt (Figure 2b). The N_A value increased from 21 to 101 mm⁻² within 10 min of N_2 gas injection as the melt achieved an N content of 58 ppm. A little increase in the N_A value of inclusions occurred in sample S3 (15 min after N_2 gas injection). Thereafter, although the N content of steel did not show much variation, the number of inclusions decreased by almost 50% after 30 min of holding, and then it remained virtually constant. Similar to the 533N-P steel, as N content of 533N-I steel increased, the N_A value of Al_2O_3 inclusions decreased to less than 1 mm⁻², and that of AlN substantially increased counting for more than 95% of the total number of inclusions. The N_A of MnS inclusions in 533N-I steel samples was also relatively small ($N_A < 5$ mm⁻²), and the N_A of ‘Other’ inclusion was negligible.

A comparison of both experiments shows that it took a longer holding time (more than 90 min) for steel to achieve the highest N content when N_2 gas was purged in the system, while the maximum N content was attained within 10 min of injecting N_2 gas into the melt. Moreover, 533N-I steel contained ~60% higher number of inclusions as compared to that of 533N-P steel for a similar N content of steel melt.

The variation in the characteristics of inclusions was further explored by analyzing the sub-classes of Al_2O_3 and AlN inclusions. In 533N-P samples, more than 90% of Al_2O_3 inclusions were $Al_2O_{3(pure)}$ and remaining were Al_2O_3 -MnS. The sample S1 from 533N-I contained 8 mm⁻² of Al_2O_3 inclusions, out of which ~60% are $Al_2O_{3(pure)}$. In the remaining samples, the percentage of $Al_2O_{3(pure)}$ varied from 20–90% of Al_2O_3 inclusions. However, the fraction of Al_2O_3 inclusions were generally insignificant in all samples except in S1 and S2 from 533N-P and S1 from 533N-I steel.

Figure 3 presents the influence of N content on the characteristics of sub-classes of AlN inclusions. AlN-MnS was the dominant sub-class before the purging of N_2 gas in 533N-P steel (Figure 3a). It made over 60% of AlN inclusions in S1, while the fractions of AlON and AlON-MnS were ~18% each. As the N content increased to 23 ppm in sample S2, a significant amount (more than 50%) of AlN_(pure) inclusions appeared, and the fraction of AlN-MnS was reduced to less than 10%. The fraction of AlON inclusions in S2 was almost 40%, and the amount of AlON-MnS was negligible. With further increase in N content in 533N-P steel, the percentage of AlN_(pure) inclusions kept on increasing at the expense of that of AlN-MnS and AlON-MnS. The AlN inclusions in sample S5 (54 ppm N) and S6 (52 ppm N) contained more than 95% of AlN_(pure) and ~5% of AlON, while ~1% of these inclusions was AlN-MnS.

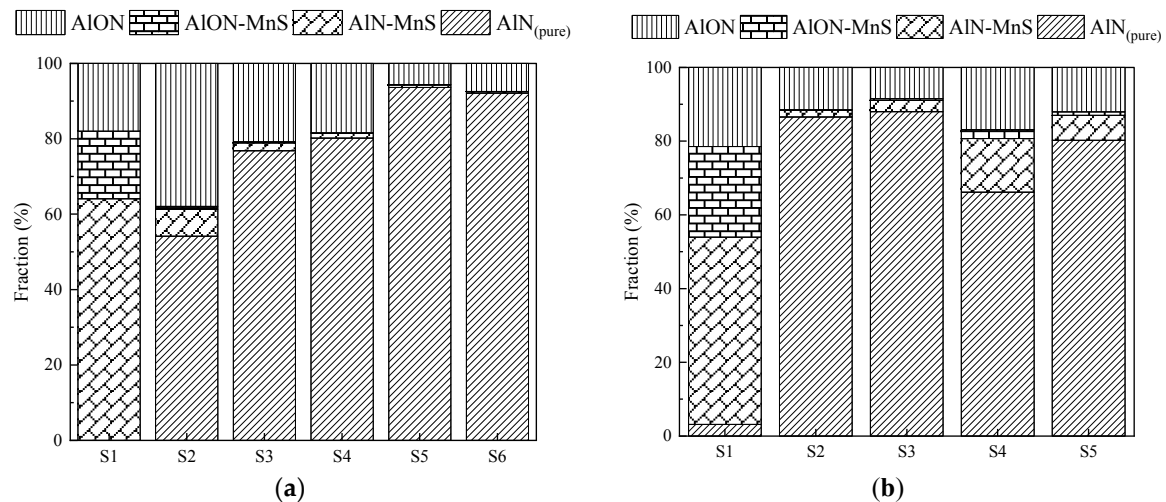


Figure 3. The fraction of subclasses of AlN inclusions for (a) 533N-P and (b) 533N-I steels.

As shown in Figure 3b, before N₂ gas injection, MnS containing nitrides (i.e., AlN-MnS and AlON-MnS) were also dominated sub-classes among others of AlN in 533N-I steel. AlN-MnS and AlON-MnS added up to ~80% of AlN inclusions. The AlN inclusions in S2 (58 ppm N) and S3 (56 ppm N) from 533N-I steel exhibited similar characteristics as those of AlN inclusions observed in S5 and S6 from 533N-P steel. AlN inclusions in these samples contained <5% MnS containing nitrides. Thereafter, despite the high N content of samples S4 and S5, the fraction of AlN-MnS and AlON-MnS inclusions increased to (~26%) and (~10%), respectively.

Though Figure 3 suggested that the fraction of AlN-MnS and AlON-MnS inclusions was significantly influenced by the N content of steel, the N_A value of these inclusions was not much affected by N content. It can be seen in Table 3 that the N_A values of AlN-MnS and AlON-MnS were consistently low ($\leq 6 \text{ mm}^{-2}$) compared to the total amount of inclusions in each sample in both steel melts.

Table 3. The N_A values of AlN-MnS and AlON-MnS inclusions in 533N-P and 533N-I steel melts.

533N-P	S1	S2	S3	S4	S5	S6
AlN-MnS (mm^{-2})	2.08	1.70	1.05	0.76	0.41	0.23
AlON-MnS (mm^{-2})	0.58	0.20	0.14	0.12	0.08	0.03
533N-I	S1	S2	S3	S4	S5	
AlN-MnS (mm^{-2})	4.57	1.78	3.20	6.58	3.10	
AlON-MnS (mm^{-2})	2.21	0.11	0.50	1.10	0.45	

4. Discussion

4.1. Thermodynamics of AlN Formation

The thermodynamic analysis was carried out to evaluate the formation behavior of AlN inclusions. The analysis aimed at determining: the critical N content required for the formation of AlN in liquid steel, the effect of temperature on the formation of AlN, and the solid fraction (g_s) values at which AlN forms during solidification.

Figure 4 presents an AlN stability diagram for the experimental steel composition of 533N-P and 533N-I, obtained by using FactSage 7.3 (FSstel, FToxid, and FactPS databases). The figure also shows AlN stability lines for different temperatures, including liquidus temperature (T_{liq}) of experimental steels. T_{liq} was around 1726.3 K, while the critical N content for the formation of AlN at 1873 K was 50 ppm for the steel melt containing 2.67% Al (average value) in the current study. Whereas, at 1823 K and 1773 K it was 30 ppm and 15 ppm, respectively. The experimental compositions plotted in Figure 4

indicate that AlN could form in liquid steel at 1873 K in sample S5 and S6 from 533N-P. The composition of S4 lay just below the 1873 K line, and those of S3 and S2 were above the 1773 K line. This indicates that AlN is not stable at 1873 K for S4, S3, and S2. However, AlN can form in liquid steel at temperatures above 1773 K during the cooling of these samples. Moreover, the composition of S1 was below the T_{liq} line, suggesting that AlN can only form in the mushy zone during solidification of S1.

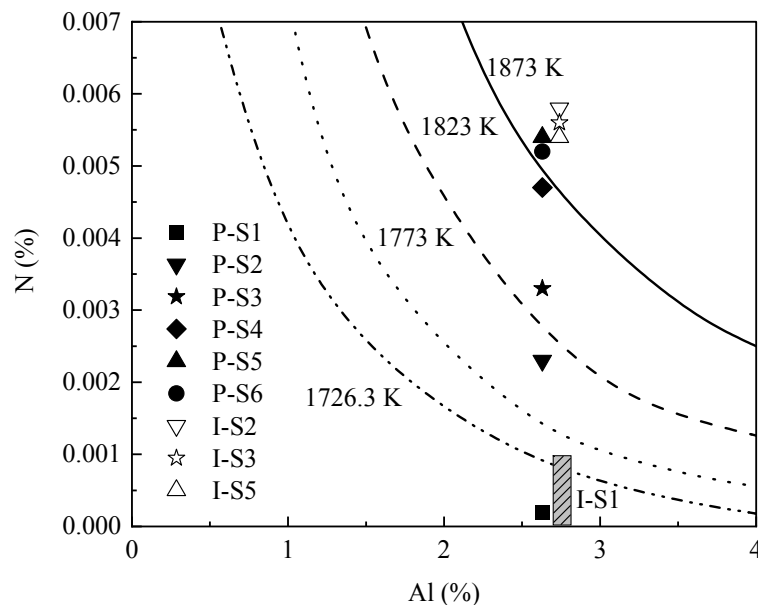


Figure 4. AlN stability diagram for the experimental steel composition of 533N-P and 533N-I, obtained by using FactSage 7.3.

For the case of 533N-I steel, AlN can form at 1873 K in all the samples, except S1. The N content of S1 was not known. However, authors have observed in previous work [15] that Fe5Mn3Si3Al steels (without N addition) contained < 10 ppm of N. Therefore, it was reasonable to assume that S1 in 533N-I steel had an N content of less than 10 ppm. This assumption would locate the S1 below the T_{liq} line in Figure 4. Thus, the AlN inclusions observed in S1 samples of both experiments were formed during solidification of the steel due to the enrichment of Al and N at the solidifying front. The enrichment led to a higher driving force for the formation of AlN. The solid fraction (g_s) values at which AlN would start to form for the S1 compositions were calculated by adopting the Scheil equation [18,29,30]. The detailed procedure for this calculation was given elsewhere [14,18]. According to the estimates, the g_s values for S1 samples should be higher than 0.11 (based on 10 ppm N), and they could be as high as 0.71 assuming 2 ppm N content.

The current steel compositions could be divided into three groups following their N contents, i.e., low N (2–10 ppm), medium N (23–47 ppm), and high N (>50 ppm) containing steels. Based on the thermodynamic analysis, it could be inferred that for low N containing steel samples, AlN inclusions formed in the mushy zone due to the segregation of Al and N at the solidification front. For both medium and high N containing samples AlN formed in the liquid steel. However, AlN formation occurred during the cooling of medium N containing samples, whereas, AlN observed in high N containing samples formed at the experimental temperature.

A variation in the characteristics of AlN inclusions in the above mentioned three groups could be expected due to the difference in the formation behavior of AlN inclusions in them. These characteristics included the number density of inclusions, their chemical composition, and their size distribution. The expected response was reflected in the results presented in Figure 3a,b.

The influence of N content on the particle size distributions (PSD) of AlN inclusions can be seen in Figure 5. In the case of low N containing samples (i.e., S1), most of the AlN inclusions lay in size range of 1–2 μm . Specifically, 92% and 80% of AlN inclusions in S1 from 533N-P and 533N-I steel melts

had $D_{ave} < 2 \mu\text{m}$, respectively. It is evident from Figure 5a that the percentage of AlN inclusions with $D_{ave} < 2 \mu\text{m}$ decreased as the N content increased in samples of 533N-P steel. In high N containing samples (S5 and S6), ~40% of AlN inclusions were greater than $2 \mu\text{m}$. Similarly, the samples with high N from the 533N-I melt (Figure 5b) contained only ~20% of AlN (except S3, which contains ~45%) in the size range of $D_{ave} < 2 \mu\text{m}$ in comparison to 80% in low N sample. A higher fraction of small-sized inclusions ($D_{ave} < 2 \mu\text{m}$) in samples with low N levels supports the inference that AlN inclusions form during solidification in these samples. Interestingly, the fraction of large-sized inclusions in high N containing samples of 533N-I was considerably higher than in those of 533N-P. This can be attributed to a higher growth rate of AlN inclusions due to turbulence induced by injection of N_2 gas in the melt. The increased size of inclusions was also reflected as a decreased number of AlN inclusions in S4 and S5 of 533N-I (Figure 2b) steel, which was probably due to the floatation of inclusions to the steel surface.

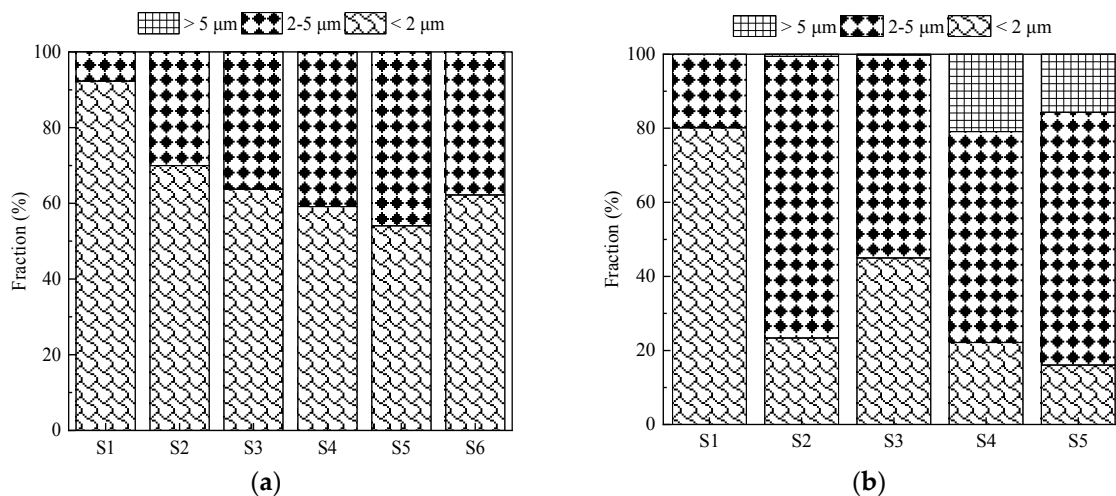


Figure 5. The particle size distribution of AlN primary class for (a) 533N-P and (b) 533N-I steels.

The thermodynamic analysis and characteristics of observed AlN inclusions also suggest that at low N levels, AlN-MnS inclusions are formed. Moreover, medium and high N levels resulted in $\text{AlN}_{(\text{pure})}$ inclusions. It could be inferred that AlN formed at the solidification front ended up having a composition of AlN-MnS, while the ones formed in liquid steel did not promote AlN-MnS formation; instead, they became $\text{AlN}_{(\text{pure})}$ inclusions. This phenomenon was investigated by considering the effect of the cooling rate and presented in the following section.

4.2. Formation of AlN Inclusions during Solidification

Samples from bulk steel had been analyzed to study the behavior of AlN at the solidification front. The bulk samples were cooled at a slow cooling rate, i.e., 0.167 K/s, as compared to 20–30 K/s [31] of air-cooled pin samples. The obtained data were compared to the results of a previous study [15]. The data of the prior research was for steel containing 5% Mn, 3% Si, 3% Al and < 10 ppm N. This steel was referred to as 533 steel in the current study. Figure 6 compares the fractions of different sub-classes of AlN inclusions observed in pin and bulk samples of 533N-P and 533 steel melts. For this comparison, the pin samples were taken before the cooling of bulk steel starts have been selected, i.e., the sample was taken at 300 min of holding time from 533N-P steel and at 41 min of holding time from 533 steel. The selection of these pin samples enabled a plausible comparison to their respective bulk samples, as in both experiments the bulk steel was exposed to similar holding time and cooling rates after these pin samples were taken.

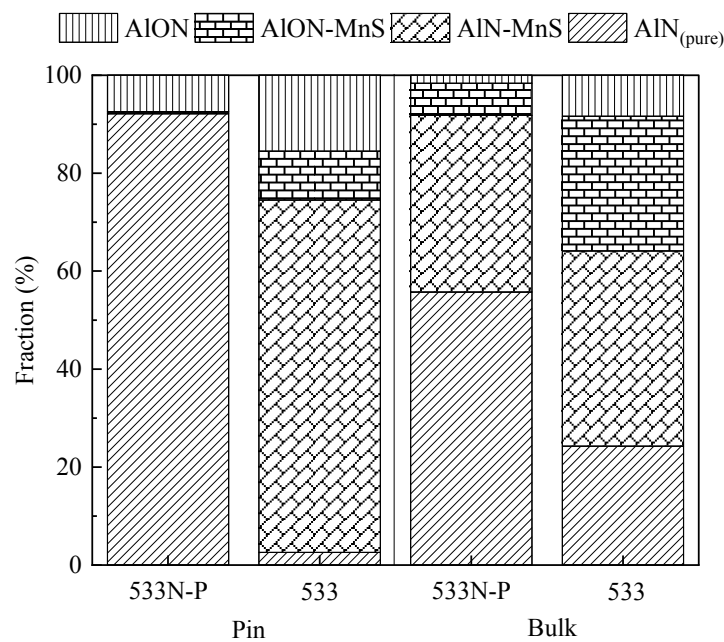


Figure 6. The fraction of AlN subclasses in the pin and bulk samples of 533N-P and 533 steel melts.

As can be seen in Figure 6, AlN_(pure) inclusions were the dominant sub-class (more than 90%) in the pin sample of 533N-P steel. Whereas, AlN-MnS made a significant portion (~80%) of AlN inclusions in 533 steel's pin sample, and the remaining were AlON (15%), AlON-MnS (5%), and a negligible amount of AlN_(pure). The fraction of AlN_(pure) inclusions decreased to ~60% in the bulk sample of 533N-P as compared to its respective pin sample. Moreover, a significant fraction (~30%) of AlN-MnS inclusions appeared in the bulk sample, and these inclusions were not present in the pin sample. On the contrary, in 533 steel melt, the slow cooling resulted in an increase (~20%) and a decrease (~30%) in the percentage of AlN_(pure) and AlN-MnS inclusions, respectively. It was interesting to see that despite a high N level in both pin and bulk samples of 533N-P steel, a substantial quantity of AlN-MnS inclusions was found in the slowly cooled bulk sample. Similarly, although 533 steel contained a low N level, its bulk sample had a considerable amount of AlN_(pure) inclusions. To understand this and elucidate the formation behavior of AlN_(pure) and AlN-MnS inclusions, two things needed to be considered: formation temperature of AlN and MnS, and capability of AlN and MnS to heterogeneously nucleate on each other.

Firstly, the formation temperature of AlN (T_{AlN}) and that of MnS (T_{MnS}), along with liquidus and solidus temperature of both 533N-P and 533 steel samples are given in Table 4. Secondly, it is known that AlN and MnS can co-precipitate together due to similarities in their crystal structures [20]. For co-precipitation, AlN can act as the nucleation site for MnS or MnS can act as the nucleation site for AlN [9].

Table 4. The temperature of liquidus, solidus, AlN, and MnS inclusion formation in the steel.

533N Steel Melt	N (%)	T_{AlN} (K)	T_{MnS} (K)	T_{liq} (K)	T_{sol} (K)
Low N	0.0002	1679.05	1472.78	1726.3	1611
Medium N	0.0023	1796.09	1473.89		
	0.0047	1865.39	1473.96		
High N	0.0054	1879.46	1473.97		

For low N level samples (533 steel), T_{AlN} was higher than T_{MnS} and lay between liquidus and solidus temperature. AlN was formed at the solidification front, which was enriched in solute elements

Al, N, Mn, and S. There was ~206 K difference between T_{AlN} and T_{MnS} . At a high cooling rate, the formation of AlN and MnS took place almost at the same time resulting in AlN-MnS inclusions. In the case of the bulk sample, the slow cooling rate facilitated the formation of $\text{AlN}_{(\text{pure})}$ at an early stage of solidification (g_s value in the range of 0.71–0.11 for $N < 10$ ppm). This occurred before the liquid steel at the solidification front became enriched in Mn and S at a level that enabled MnS formation. However, the AlN inclusions formed at the end of solidification, closer to Mn and S segregated region, became sites for heterogeneous nucleation of MnS and eventually had a composition of AlN-MnS inclusions.

In the case of a pin sample from 533N-P, a higher difference (~405 K) between T_{AlN} and T_{MnS} resulted in the formation of a higher fraction of $\text{AlN}_{(\text{pure})}$ inclusions. When this high N containing steel solidified at a slow rate, $\text{AlN}_{(\text{pure})}$ inclusions formed in liquid steel at 1873 K until the start of solidification and at the early stage of solidification, and AlN-MnS inclusions formed at the end of solidification.

According to the above discussion and in Section 4.1, the AlN-MnS should always form due to segregation at the end of solidification. The fraction of AlN-MnS inclusions appeared to be very low in the pin sample of 533N-P (Figure 6); however, as shown in Table 3, there was a similar amount (N_A) of AlN-MnS present in all the pin samples of 533N-P. It is to mention that a scatter was observed in the N_A of AlN-MnS inclusions in the pin samples taken at different holding times during an experiment. This scatter could be caused by a difference in the mass of the sample, leading to some variation in the cooling rate of the individual pin sample. However, it appeared that the N content of steel did not influence the amount of AlN-MnS inclusions in samples taken during an experiment. For instance, the N_A value of AlN-MnS inclusions in low N sample (S1) of 533N-I was $\sim 4.5 \text{ mm}^{-2}$, whereas S4 and S5 (high N samples) contained $\sim 6.5 \text{ mm}^{-2}$ and $\sim 3 \text{ mm}^{-2}$ of AlN-MnS inclusions. The N_A of AlN-MnS inclusions in low and high N samples (S1 and S4) of 533N-P was $\sim 2 \text{ mm}^{-2}$ and $\sim 0.8 \text{ mm}^{-2}$, respectively. Hence, there was no apparent influence of N content on the amount of AlN-MnS inclusions. This was in agreement with the explanation that AlN-MnS inclusions were formed at solidification front enriched with Mn and S and that their amount depended on the cooling rate.

As mentioned, AlN and AlN-MnS inclusions were the common types of inclusions present in the current experimental steels. Few studies [32,33] have focused on the influence of AlN and AlN-MnS inclusions on the mechanical properties of the steel. AlN inclusions could be found both inside the grain [34] or at the grain boundaries [32,34]. However, the AlN inclusions were reported to be more detrimental when they were located at the grain boundaries. Kang et al. [32] studied the hot ductility on the twinning-induced plasticity (TWIP) steels and observed that AlN inclusions precipitated at the austenite grain boundaries promoted the poor ductility of the steel. The AlN inclusions that precipitate at grain boundaries usually combine with MnS to form AlN-MnS due to the ease of co-precipitation of AlN and MnS to occur. Ushioda et al. [33] observed that AlN-MnS inclusions formed in the austenite grain boundaries in low carbon steel and reported that the complex precipitation of AlN and MnS is harmful to the hot ductility of the steel. The current study suggests that the N content of steel did not influence the amount of AlN-MnS inclusions. However, this inference is based on fast cooled pin samples and inclusions having a $D_{\text{ave}} > 2 \mu\text{m}$. In the case of slow-cooled samples, the N content of steel could influence the amount of AlN-MnS inclusions, i.e., a higher N content could result in a higher number of AlN-MnS inclusions especially considering that the AlN inclusions could be pushed to the solidification front during solidification of steel.

The formation of AlON and AlON-MnS took place as follows. First Al_2O_3 inclusions were formed in the liquid steel, as they were stable at 1873 K. It was followed by the formation of AlN inclusions when the N content in the steel was sufficient for AlN formation. AlON could be a result of AlN precipitation on Al_2O_3 or collision of AlN and Al_2O_3 particles. The precipitation of AlN on Al_2O_3 is possible, but on specific crystallographic orientations [35], therefore, the number of observed AlON inclusions was small. Similar to AlN-MnS, the formation of AlON-MnS occurred during the

solidification process, where either Al_2O_3 and/or AlN in AlON inclusion became the nucleation site for MnS inclusion.

4.3. Co-Precipitation of Inclusions

In the current study, the formation of complex inclusions (AlN-MnS , $\text{Al}_2\text{O}_3\text{-MnS}$, and AlON) mostly occurred due to co-precipitation. The co-precipitation behavior can be quantified by considering precipitation ratio (PR) of one phase on another. The PR of phase 1 on phase 2 to form co-precipitates is defined as the ratio of the number of co-precipitates to the sum of the number of phase 2 particles and co-precipitates. The PR value is related to the potency of a phase to act as a heterogeneous nucleation site for others. In a previous study [15], the authors compared the PR values of MnS on AlN and Al_2O_3 for the formation of AlN-MnS and $\text{Al}_2\text{O}_3\text{-MnS}$ co-precipitates, respectively. It was reported that the PR value of MnS on AlN was always higher than that on Al_2O_3 due to a low mismatch between MnS and AlN (~5%) [36] as compared to that of MnS and Al_2O_3 (~12%) [36]. However, that was based on low N containing steels. In the current study, it was observed that the PR values of AlN containing co-precipitates could be influenced by the N content of the steel.

Figure 7 shows a comparison of the PR values of MnS on AlN and Al_2O_3 observed in the previous study [15] (533 steel), which had low N content and the present study for 533N-P, which has low, medium, and high N containing samples. In the case of the PR value of MnS on AlN inclusions, in the low N content (533 and S1 of 533N-P), the PR value was more than 98%. However, in the medium (S2–S4) and high (S5 and S6) N containing samples, the PR values were significantly low, less than 15%. On the other hand, the PR values of MnS on Al_2O_3 were always less than 15% and were not influenced by the N content of the steel. It appeared that for samples having medium and high N content, the MnS PR values could be higher for Al_2O_3 as compared to for AlN . However, it should be noted that the lower PR values in medium and high N containing samples did not indicate that MnS prefers to nucleate on Al_2O_3 . The lower MnS PR values on AlN were due to the formation of $\text{AlN}_{(\text{pure})}$ in liquid steel.

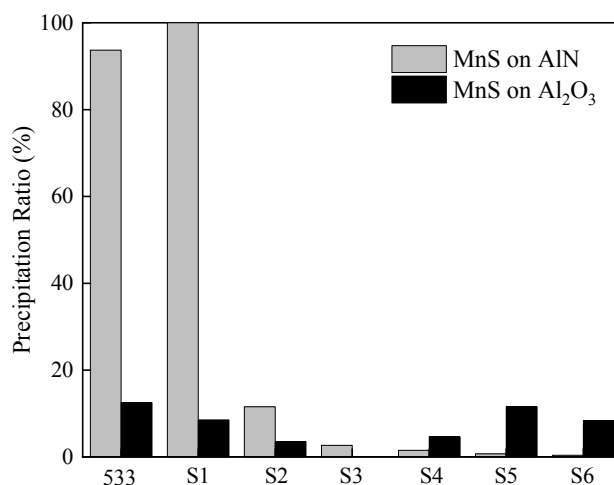


Figure 7. A comparison of the MnS precipitation ratio (PR) values for AlN and Al_2O_3 inclusions.

The N content also influenced the PR values of AlN on Al_2O_3 to form AlON . Figure 8 shows the AlN PR values observed in 533 [15] and 533N-P. The low N containing samples (533 and S1 from 533N-P) had PR values of less than 20%. As the N content in the steel increased (S2–S6), the PR values increased dramatically to over 80%. This implied that more AlN inclusions were available to co-precipitate with $\text{Al}_2\text{O}_{3(\text{pure})}$ to form AlON inclusion.

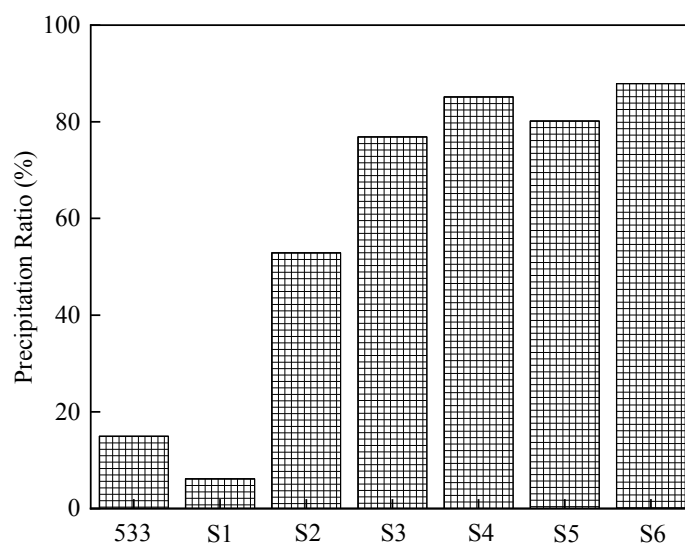
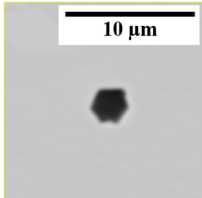
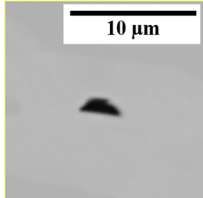
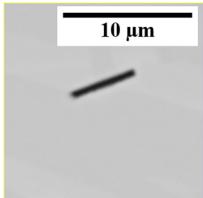
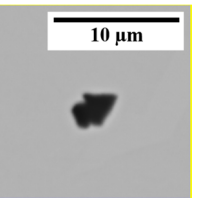
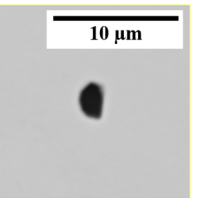


Figure 8. The precipitation ratio (PR) value for AlN on $\text{Al}_2\text{O}_3(\text{pure})$ inclusions on 533N-P steels.

4.4. Effect of N Content on the Morphology of $\text{AlN}_{(\text{pure})}$ Inclusions

In this study, the $\text{AlN}_{(\text{pure})}$ inclusions were classified into five types based on their morphology, as displayed in Table 5. The inclusions having 5 or 6 sides were grouped as a plate-like type, and those with 3 or 4 sides were classified as angular. The inclusions exhibiting a long and thin morphology were grouped as a needle-like type. Agglomerates represented inclusions that consist of two or more particles. The remaining inclusions had irregular morphology.

Table 5. Morphologies of $\text{AlN}_{(\text{pure})}$ inclusions.

Plate-like	Angular	Needle	Agglomerate	Irregular
				

The low N containing sample (S1) from 533N-P did not contain any $\text{AlN}_{(\text{pure})}$ inclusions, and that from 533N-I contained only 4 $\text{AlN}_{(\text{pure})}$ inclusions, which were all angular. The morphology of $\text{AlN}_{(\text{pure})}$ inclusions observed in the medium and high N containing samples of both steel melts was shown in Figure 9a,b, respectively. In 533N-P samples, around 70% of $\text{AlN}_{(\text{pure})}$ inclusions have angular morphology. A small fraction (~6%) of inclusions with needle shape was found in samples containing medium N levels (S3 and S4). The number of plate-like inclusions was relatively higher in high N samples, i.e., around 14–18%, as compared to 8–9% in medium N samples. Approximately 6–13% inclusions were agglomerate, while irregular morphology makes 4–13%. In the case of 533N-I steel samples, plate-like morphology was a dominating type (36–60%). It was followed by an angular type that is around 26–36%. The fraction of agglomerate inclusions increased from 11 to 32% with increased holding time (S2 to S4) and then decreased to 19% in sample S5. The needle and irregular shaped inclusions were present in small amounts, i.e., 4–10% and ~2%, respectively.

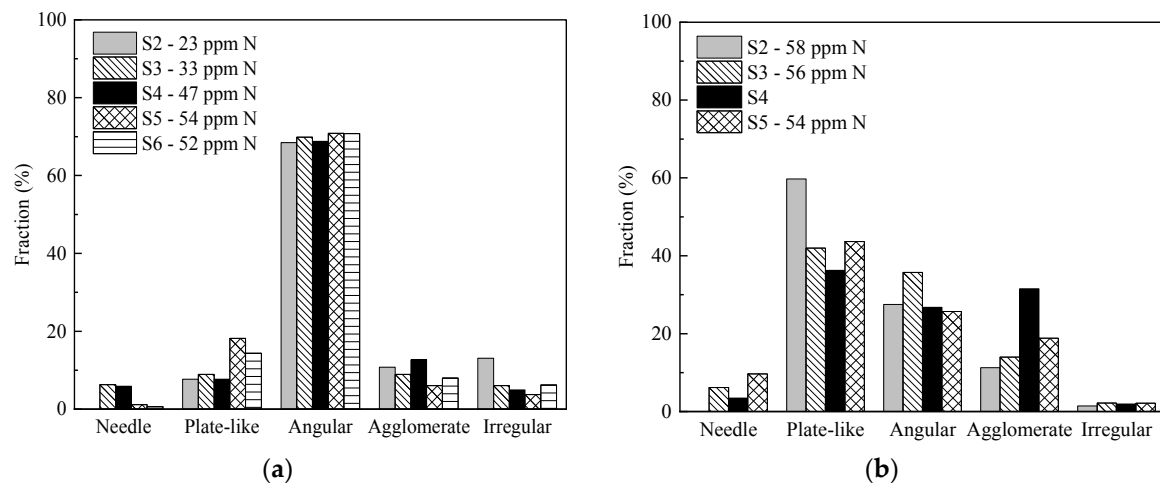


Figure 9. The fraction of morphology of $\text{AlN}_{(\text{pure})}$ inclusions in (a) 533N-P and (b) 533N-I steel melts.

It is of interest to observe a higher fraction of plate-like inclusions in samples with high N content. It could be related to the stability of AlN at 1873 K for high N containing samples. The effect of N content was observed in both experimental steel melts; moreover, the fraction of plate-like inclusions in 533N-I was significantly higher than that observed in S5 and S6 of 533N-P steel. This could be due to fast kinetics conditions in this steel. The turbulent conditions could lead to a faster growth rate of inclusions, enabling them to be detected under settings of current inclusion analysis ($D_{\text{ave}} > 2 \mu\text{m}$).

Moreover, a few samples were electrolytically etched in a 10% AA (10 v/v% acetylacetone – 1 w/v% tetramethylammonium chloride – methanol) electrolyte to expose three-dimensional morphology of inclusions. It was found that a considerable number of AlN inclusions were oriented at different angles to the analyzed surface. Such orientation of plate-like inclusions could make them appear as angular inclusions on a two-dimensional surface. Figure 10 shows examples of such inclusions. It was clear from secondary electron images (SEI) (Figure 10a) that the observed inclusions are, in fact, plate-like in shape. While from the back-scattered electron (BSE) images (Figure 10b), they could be defined as angular inclusions, especially if the surface had been polished.

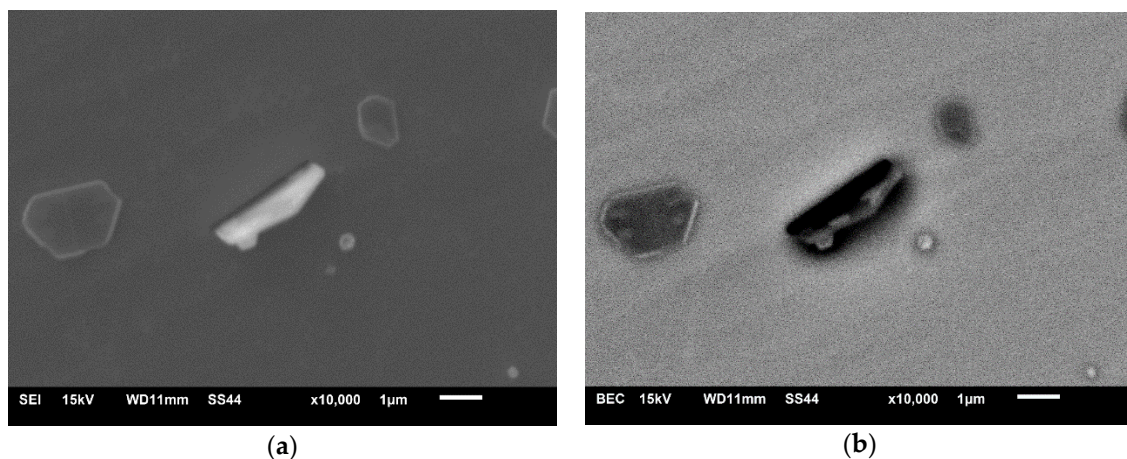


Figure 10. (a) Secondary electron images (SEI) and (b) back-scattered electron (BSE) images of AlN inclusions which are positioned in a different angle.

Applying the same reasoning, it could be argued that there is a possibility that inclusions with needle morphology could also be plate-like when observed in three-dimensions. To clarify this, the maximum diameter (D_{max}) of plate-like and needle inclusions observed in S4 and S5 of 533N-P steel was compared and shown in Figure 11. It could be seen that the D_{max} values of plate-like inclusion

varied from 1 to 5 μm (Figure 11a). Whereas needle-shaped inclusions had D_{max} values in the range of 3 to 10 μm , and more than 90% of them were larger than 5 μm (Figure 11b). It is evident from Figure 11 that needle-shaped inclusions were not plate-like inclusions oriented at an angle as the D_{max} values of needle-shaped inclusions were significantly higher than those of plate-like inclusions.

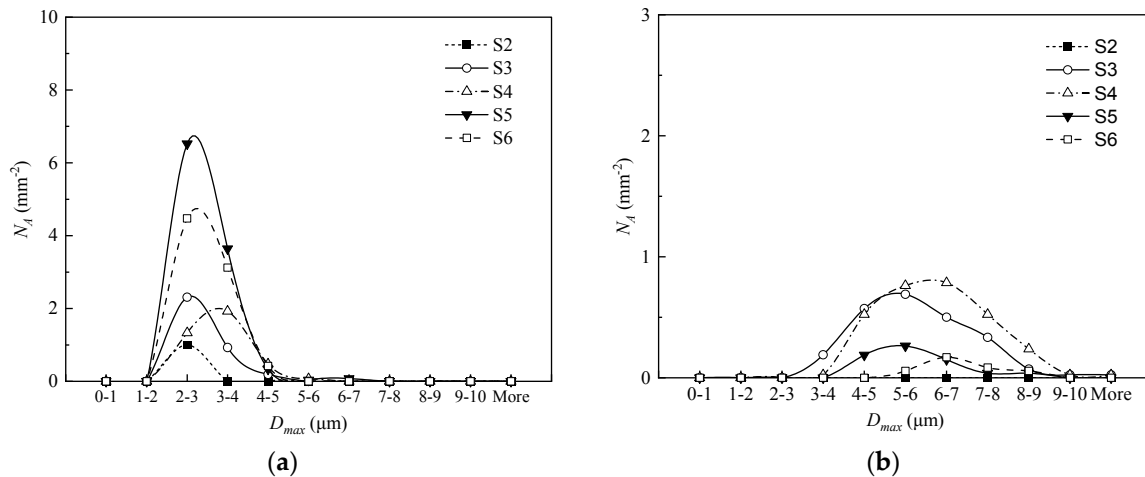


Figure 11. The size distribution of the AlN inclusions with (a) the plate-like and (b) needle shape in 533N-P steel samples.

Based on Figure 9 through Figure 11, AlN inclusions were detected in various morphologies. A similar observation was made by previous researchers [3,4,9,20]. Tuling and Mintz [20] investigated the morphology of AlN inclusions in high Al transformation induced plasticity (TRIP) steels with 2.5% Mn, 60–70 ppm N, and 1–1.5% Al. According to the thermodynamics, AlN inclusions were formed during solidification for both 1% and 1.5% Al containing TRIP steels. Dendritic and hexagonal (plate-like) AlN inclusions were observed in steel with 1% Al and 1.5% Al, respectively. Liu et al. [4] reported plate-like morphology of single AlN inclusions in the twin-induced plasticity (TWIP) steel (Fe-18Mn-1.5Al with 78 ppm N) and suggested that these AlN inclusions were formed above the T_{liq} of the investigated steel. Wang et al. [3] detected fine particles of AlN inclusions at the grain boundaries of TWIP steel (Fe-16Mn-0.54Al) with 63 ppm N content and coarse hexagonal (plate-like) AlN particles at the fracture site of TWIP steel (Fe-17Mn-2.1Al) with 43 ppm N content. For both these compositions of steel, thermodynamically AlN should form during solidification i.e., below the T_{liq} . Moreover, Kang et al. [9] suggested that the presence of MnS inclusions can affect the morphology of AlN inclusions. They observed AlN inclusions in high Al TWIP steel (Fe-18Mn-1.5Al and 80–93 ppm N) with different sulfur content. It was reported that in the absence of MnS inclusions i.e., when the steel had 32 ppm S, the AlN inclusions had hexagonal (plate-like) shape. In case of an abundance of MnS (S content up to 100–230 ppm), AlN inclusions exhibited dendritic and hexagonal (plate-like) morphologies. Based on thermodynamics, AlN inclusions would have formed during solidification for all the compositions investigated by Kang et al. [9]. From the above mentioned literature it can be seen that AlN inclusions can exhibit various morphologies regardless of whether they are formed during solidification or above T_{liq} . Similar behavior is observed in the current study. A three-dimensional inclusion analysis is recommended for further investigation.

5. Conclusions

The influence of N content on the characteristics of inclusions in Fe-5Mn-3Al-3Si steel was investigated in the current study. Nitrogen was added into liquid steel by purging the N_2 gas into the atmosphere of a sealed furnace containing molten steel or by directly injecting N_2 gas into the molten steel. The steel compositions were divided into three groups based on their N levels, i.e., low N

(<10 ppm), medium N (23–47 ppm), and high N (>50 ppm) containing steels. The following findings are obtained:

- (1) A high N content of steel can be achieved in a short time by injection of N₂ gas into the melt.
- (2) The number of inclusions increased from ~13 mm⁻² to ~64 mm⁻² as N content increased from low to medium level, as observed in 533N-P steels. The number of inclusion remained constant by a further increase in N content. However, in the case of 533N-I steels, the number of inclusion increased up to 108 mm⁻² at the high level of N content.
- (3) In low N content steel, AlN-MnS inclusions were dominating class (40–60% of the total inclusions). While in medium and high N content steel samples, AlN_(pure) inclusions are the primary class of inclusions (50–90% of the total inclusions).
- (4) The number of AlN-MnS inclusions is not affected by the N content of steel as they are formed during solidification. However, the cooling rate has an influence on their number.
- (5) The amount of Al₂O₃ inclusions decreases with an increase in the N content of the steel. Low N samples contained 10 mm⁻² of Al₂O₃ inclusions, which decreased to 2 mm⁻² and 1 mm⁻² in medium and high N containing samples, respectively.
- (6) AlN inclusions exhibit different morphologies such as plate-like, needle-like, angular, and agglomerates. Three-dimensional observation of angular AlN inclusions showed that they could be plate-like inclusions which are positioned at different orientations, making them appear angular.
- (7) Since the morphological information can be misinterpreted in a two-dimensional observation, a three-dimensional inclusion analysis is recommended for detailed morphological investigation of AlN inclusions.

Author Contributions: Conceptualization, M.A. and N.D.; methodology, M.A. and M.N.; software, M.A.; formal analysis, M.A.; investigation, M.A.; writing—original draft preparation, M.A.; writing—review and editing, M.A., M.N. and N.D.; supervision, N.D.; project administration, N.D.; funding acquisition, N.D. All authors have read and agreed to the published version of the manuscript.

Funding: This research was funded by Natural Sciences and Engineering Research Council of Canada, Project Number 20007079.

Acknowledgments: The authors would like to express gratitude to Stanley Sun and Li Sun at ArcelorMittal Dofasco for their valuable time and fruitful discussions. Further, we also want to thank the Canadian Centre for Electron Microscopy (CCEM) for providing access to the JEOL 6610 to conduct the scanning electron microscopy analysis.

Conflicts of Interest: The authors declare no conflict of interest. The funders had no role in the design of the study; in the collection, analyses, or interpretation of data; in the writing of the manuscript, or in the decision to publish the results.

References

1. Hu, B.; Luo, H.; Yang, F.; Dong, H. Recent progress in medium-Mn steels made with new designing strategies, a review. *J. Mater. Sci. Technol.* **2017**, *33*, 1457–1464. [[CrossRef](#)]
2. Steenken, B.; Rezende, J.L.L.; Senk, D. Hot ductility behaviour of high manganese steels with varying aluminium contents. *Mater. Sci. Technol.* **2017**, *33*, 567–573. [[CrossRef](#)]
3. Wang, Y.-N.; Yang, J.; Wang, R.-Z.; Xin, X.-L.; Xu, L.-Y. Effects of Non-metallic Inclusions on Hot Ductility of High Manganese TWIP Steels Containing Different Aluminum Contents. *Metall. Mater. Trans. B* **2016**, *47*, 1697–1712. [[CrossRef](#)]
4. Liu, H.; Liu, J.; Wu, B.; Shen, Y.; He, Y.; Ding, H.; Su, X. Effect of Mn and Al contents on hot ductility of high alloy Fe-xMn-C-yAl austenite TWIP steels. *Mater. Sci. Eng. A* **2017**, *708*, 360–374. [[CrossRef](#)]
5. Kong, L.; Deng, Z.; Zhu, M. Formation and Evolution of Non-metallic Inclusions in Medium Mn Steel during Secondary Refining Process. *ISIJ Int.* **2017**, *57*, 1537–1545. [[CrossRef](#)]
6. Yu, Z.; Liu, C. Modification mechanism of spinel inclusions in medium manganese steel with rare earth treatment. *Metals (Basel)* **2019**, *9*, 804. [[CrossRef](#)]
7. Grajcar, A.; Woźniak, D.; Kozłowska, A. Non-Metallic Inclusions and Hot-Working Behaviour of Advanced High-Strength Medium-Mn Steels. *Arch. Metall. Mater.* **2016**, *61*, 811–820. [[CrossRef](#)]

8. Yu, Z.; Liu, C. Evolution Mechanism of Inclusions in Medium-Manganese Steel by Mg Treatment with Different Aluminum Contents. *Metall. Mater. Trans. B Process Metall. Mater. Process. Sci.* **2019**, *50*, 772–781. [[CrossRef](#)]
9. Kang, S.E.; Banerjee, J.R.; Mintz, B. Influence of S and AlN on hot ductility of high Al, TWIP steels. *Mater. Sci. Technol.* **2012**, *28*, 589–596. [[CrossRef](#)]
10. Thornton, P.A. The influence of nonmetallic inclusions on the mechanical properties of steel: A review. *J. Mater. Sci.* **1971**, *6*, 347–356. [[CrossRef](#)]
11. Maciejewski, J. The Effects of Sulfide Inclusions on Mechanical Properties and Failures of Steel Components. *J. Fail. Anal. Prev.* **2015**, *15*, 169–178. [[CrossRef](#)]
12. Ånmark, N.; Karasev, A.; Jönsson, P. The Effect of Different Non-Metallic Inclusions on the Machinability of Steels. *Materials (Basel)* **2015**, *8*, 751–783. [[CrossRef](#)] [[PubMed](#)]
13. Tomita, Y. Effect of morphology of nonmetallic inclusions on tensile properties of quenched and tempered 0.4C-Cr-Mo-Ni steel. *Mater. Charact.* **1995**, *34*, 121–128. [[CrossRef](#)]
14. Alba, M.; Nabeel, M.; Dogan, N. Investigation of Inclusion Formation in Light-Weight Fe–Mn–Al Steels using Automated Scanning Electron Microscope Equipped with Energy-Dispersive X-Ray Spectroscopy. *Steel Res. Int.* **2019**, *91*, 1900477. [[CrossRef](#)]
15. Alba, M.; Nabeel, M.; Dogan, N. Effect of aluminium content on the formation of inclusions in Fe–5Mn–xAl steels. *Ironmak. Steelmak.* **2020**. [[CrossRef](#)]
16. Paek, M.-K.; Jang, J.-M.; Do, K.-H.; Pak, J.-J. Nitrogen Solubility in High Manganese-Aluminum Alloyed Liquid Steels. *Met. Mater. Int.* **2013**, *19*, 1077–1081. [[CrossRef](#)]
17. Jang, J.-M.; Paek, M.-K.; Pak, J.-J. Thermodynamics of Nitrogen Solubility and AlN Formation in Multi-Component High Mn Steel Melts. *ISIJ Int.* **2017**, *57*, 1821–1830. [[CrossRef](#)]
18. Liu, H.; Liu, J.; Michellic, S.K.; Wei, F.; Zhuang, C.; Han, Z.; Li, S. Characteristics of AlN inclusions in low carbon Fe–Mn–Si–Al TWIP steel produced by AOD-ESR method. *Ironmak. Steelmak.* **2016**, *43*, 171–179. [[CrossRef](#)]
19. Xin, X.L.; Yang, J.; Wang, Y.N.; Wang, R.Z.; Wang, W.L.; Zheng, H.G.; Hu, H.T. Effects of Al content on non-metallic inclusion evolution in Fe–16Mn– x Al–0.6C high Mn TWIP steel. *Ironmak. Steelmak.* **2016**, *43*, 234–242. [[CrossRef](#)]
20. Tuling, A.; Mintz, B. Crystallographic and morphological aspects of AlN precipitation in high Al, TRIP steels. *Mater. Sci. Technol.* **2016**, *32*, 568–575. [[CrossRef](#)]
21. Liu, H.; Liu, J.; Michellic, S.K.; Shen, S.; Su, X.; Wu, B.; Ding, H. Characterization and Analysis of Non-Metallic Inclusions in Low-Carbon Fe–Mn–Si–Al TWIP Steels. *Steel Res. Int.* **2016**, *87*, 1–10. [[CrossRef](#)]
22. Hsiao, C. Fine Aluminium Nitride Precipitates in Steel. *Nature* **1958**, *181*, 1527–1528. [[CrossRef](#)]
23. Wilson, F.G.; Gladman, T. Aluminium nitride in steel. *Int. Mater. Rev.* **1988**, *33*, 221–286. [[CrossRef](#)]
24. Li, X.; Wang, M.; Bao, Y.; Gong, J.; Wang, X.; Pang, W. Precipitation Behavior of AlN in High-Magnetic-Induction Grain-Oriented Silicon Steel Slab. *JOM* **2019**, *71*, 3135–3141. [[CrossRef](#)]
25. Croft, N.H.H.; Entwisle, A.R.R.; Davies, G.J.J. Origins of dendritic AlN precipitates in aluminium-killed-steel castings. *Met. Technol.* **1983**, *10*, 125–129. [[CrossRef](#)]
26. LECO Corp. *Oxygen and Nitrogen Determination in Refractory Metals and Their Alloys*; LECO Corporation: Saint Joseph, MI, USA, 2020; pp. 1–2.
27. LECO Corp. *Carbon and Sulfur Determination in Low Carbon Ferroalloys*; LECO Corporation: Saint Joseph, MI, USA, 2018; pp. 1–3.
28. FEI. *ASPEX Explorer-Automated Industrialized SEM with OmegaMax EDX Technology*; FEI Company: Fremont, CA, USA, 2014; pp. 1–2.
29. Paek, M.; Jang, J.; Jiang, M.; Pak, J. Thermodynamics of AlN Formation in High Manganese-Aluminum Alloyed Liquid Steels. *ISIJ Int.* **2013**, *53*, 973–978. [[CrossRef](#)]
30. Nabeel, M.; Alba, M.; Karasev, A.; Jönsson, P.G.; Dogan, N. Characterization of Inclusions in 3rd Generation Advanced High-Strength Steels. *Metall. Mater. Trans. B* **2019**, *50*, 1674–1685. [[CrossRef](#)]
31. Ericsson, O.T.; Lionet, M.; Karasev, A.V.; Inoue, R.; Jönsson, P.G. Changes in inclusion characteristics during sampling of liquid steel. *Ironmak. Steelmak.* **2011**, *39*, 67–75. [[CrossRef](#)]
32. Kang, S.E.; Tuling, A.; Banerjee, J.R.; Gunawardana, W.D.; Mintz, B. Hot ductility of TWIP steels. *Mater. Sci. Technol.* **2011**, *27*, 95–100. [[CrossRef](#)]

33. Ushioda, K.; Suzuki, H.G.; Komatsu, H.; Esaka, K. Influence of sulfur on AlN precipitation during cooling after solidification and resulting hot shortness in low carbon steel. *Nippon Kinzoku Gakkaishi J. Jpn. Inst. Met.* **1995**, *59*, 373–380. [[CrossRef](#)]
34. Chen, Y.-L.; Wang, Y.; Zhao, A.-M. Precipitation of AlN and MnS in Low Carbon Aluminium-Killed Steel. *J. Iron Steel Res. Int.* **2012**, *19*, 51–56. [[CrossRef](#)]
35. Li, F.; Li, H.; Huang, D.; Zheng, S.; You, J. Mechanism of MnS Precipitation on Al₂O₃–SiO₂ Inclusions in Non-oriented Silicon Steel. *Met. Mater. Int.* **2018**, *24*, 1394–1402. [[CrossRef](#)]
36. Ohta, H.; Suito, H. Precipitation and Dispersion Control of MnS by Deoxidation Products of ZrO₂, Al₂O₃, MgO and MnO–SiO₂ Particles in Fe–10mass%Ni Alloy. *ISIJ Int.* **2006**, *46*, 480–489. [[CrossRef](#)]



© 2020 by the authors. Licensee MDPI, Basel, Switzerland. This article is an open access article distributed under the terms and conditions of the Creative Commons Attribution (CC BY) license (<http://creativecommons.org/licenses/by/4.0/>).